electronic reprint

Acta Crystallographica Section A
Foundations of Crystallography
ISSN 0108-7673

Strength tuning of multiple waves in crystals

S. L. Morelhão and L. H. Avanci

Acta Crystallographica Section A
Foundations of Crystallography
ISSN 0108-7673

Received 12 August 2000
Accepted 31 October 2000

Strength tuning of multiple waves in crystals

S. L. Morelhão* and L. H. Avanci

Instituto de Física, USP, CP 66318, 05508-900 São Paulo, SP, Brazil. Correspondence e-mail: morelhao@if.usp.br

In this work, the linear polarization of synchrotron radiation is explored as a tuning key for the strength of the simultaneously diffracted X-ray waves in crystals. The relative strength of the waves has been defined by the reflectivities of the Bragg reflections involved in each multiple-diffraction case and it has limited the applicability of the multiple-diffraction phenomenon. With a proper choice of the wavelength and the polarization direction of the incident synchrotron radiation, it is demonstrated how the intensity ratios of the simultaneously diffracted beams can be drastically changed.

1. Introduction

Propagation of multiple waves in crystals is a phenomenon better know as *N*-beam diffraction of X-rays in crystals. Since it was observed by Renninger (1937), a considerable amount of work has been performed by several authors in order to understand the phenomenon and use it as a tool for material analysis (for example, Lipscomb, 1949; Hart & Lang, 1961; Moon & Shull, 1964; Colella, 1974; Caticha-Ellis, 1975; Post, 1977; Chang, 1982, 1984, 1998; Kshevetskii *et al.*, 1985; Thorkildsen, 1987; Shen & Collela, 1988; Shen & Finkelstein, 1992, 1993; Morelhão & Cardoso, 1996; Weckert & Hümmer, 1997; Avanci *et al.*, 1998; Avanci & Morelhão, 2000). In this work, we explore the linear polarization of synchrotron radiation as a tuning key for the strength of simultaneously diffracted waves. The relative strength of the waves has always been exclusively defined by the reflectivity of the Bragg reflections involved in each multiple diffraction case, and it has limited the applicability of the phenomenon. Simple theoretical considerations are developed to demonstrated how the intensity ratios of the simultaneously diffracted beams can be drastically changed by combining the wavelength (λ) and the polarization direction of the incident synchrotron radiation. As a practical application, three-beam diffractions with high sensitivity to the polarization direction are used to propose a method for measuring the linear polarization of an X-ray beam from a single azimuthal scan.

1.1. Polarization-forbidden reflections

For linearly polarized radiation, besides the angle of the scattering direction (2θ in Fig. 1), the intensity of coherent scattering also depends on the angle between the electric field oscillation direction and the incidence plane (χ in Fig. 1). From the classical Maxwell equations of the electromagnetism, it is understood that an accelerated charge does not irradiate in the direction of its acceleration. Then, no coherent scattering is expected at $2\theta = \pi/2$ when the electric field vector lies in the incidence plane, *i.e.* π-polarized photons ($\chi = 0$) are not coherently scattered at $\pi/2$. The dynamical theory of X-ray diffraction in crystals, which is the solution of the Maxwell equations in a medium with periodic electron density, confirms that reflections with Bragg angle of $\pi/4$ do not diffract π-polarized X-ray photons. Hereafter, reflections under such particular conditions are called polarization-forbidden reflections.

1.2. Three-beam diffraction

A crystal can be set in a position that a monochromatic beam simultaneously fulfils the diffraction condition for several Bragg reflections. By taking **P** and **S** as two reflections simultaneously diffracting the incident beam (**k**, wavevector), the diffracted beam from each reflection ($\mathbf{k}_S$ or $\mathbf{k}_P$ in Fig. 2) is formed by the waves from the reflection itself, the primary reflection, plus the waves from the detour reflection (Shen & Finkelstein, 1993; Morelhão & Abramof, 1999). For instance, if **P** is assumed to be the primary reflection, the detour reflection $\mathbf{S} + \mathbf{C}$ generates waves that have been first diffracted by the secondary reflection **S**, and re-diffracted towards the primary-beam direction by the coupling reflection[1] **C**, where $\mathbf{C} = \mathbf{P} - \mathbf{S}$. This description of a detour reflection is the second-order Born approximation for the three-beam diffraction (Shen & Collela, 1988; Chang & Tang, 1988), which is very useful for physically understanding the phenomenon. However, it is limited to the *Umweganregung* cases of multiple diffraction, those in which the primary reflection is weaker than, or comparable to, the detour reflection. The others, the *Aufhellung* cases (Wagner, 1923), are in general observed for strong primary reflections. In these cases, the contribution of the detour reflection is not enough to transfer a significant amount of intensity taken from the incident beam by the secondary reflection and/or from the primary beam by the $\bar{\mathbf{C}} = \mathbf{S} - \mathbf{P}$ reflection.

[1] The term 'coupling reflection' is used throughout this paper. Readers should note that it is not a reflection of the incident beam. It stands for the reciprocal-lattice vector **C**, which is responsible for coupling the wavefields due to **P** and **S** reflections.

2. Theory

2.1. Polarization-forbidden detour reflections

There are two distinct situations in which the detour reflection can be forbidden by polarization, *i.e.* a polarization-forbidden detour reflection. These situations occur when one of the two reflections, the secondary or the coupling reflection, is forbidden by the polarization. In each case, the Bragg angle of one of these reflections must be $\pi/4$ or very close to this value. In other words, the secondary-beam direction must be $\pi/2$ from the incident beam ($\mathbf{k}_S \cdot \mathbf{k} = 0$) or from the primary beam ($\mathbf{k}_S \cdot \mathbf{k}_P = 0$). Then, when one of these conditions is fulfilled, the wavefield contribution of the detour reflection will be eliminated at specific polarization directions (Stetsko *et al.*, 2000).

2.1.1. Polarization-forbidden secondary reflection. For a secondary reflection with Bragg angle of $\pi/4$ ($\theta_S = 45^\circ$), the polarization-forbidden detour reflection occurs when the electric field oscillation direction ($\hat{\mathbf{e}}$) of the incident X-ray beam coincides with the direction of the secondary beam. According to the reciprocal-space Ewald construction in Fig. 2, it corresponds to a rotation of the primary incidence plane (χ rotation) until the γ angle reaches zero. By defining χ equal to zero when the polarization direction lies in the incident plane, $\hat{\mathbf{e}} = \cos\chi\hat{\boldsymbol{\pi}} + \sin\chi\hat{\boldsymbol{\sigma}}$ and $\chi_{\rm pf} = \cos^{-1}(\lambda\mathbf{k}_S \cdot \hat{\boldsymbol{\pi}})$ is the value for a polarization-forbidden secondary (or detour) reflection. The unit vectors are $\hat{\boldsymbol{\sigma}} = \mathbf{k} \times \mathbf{k}_P/|\mathbf{k} \times \mathbf{k}_P|$ and $\hat{\boldsymbol{\pi}} = \lambda(\hat{\boldsymbol{\sigma}} \times \mathbf{k})$.

2.1.2. Polarization-forbidden coupling reflection. It is more difficult to obtain an analytical expression for $\chi_{\rm pf}$ when the Bragg angle of the coupling reflection is the only angle equal to or near $\pi/4$ ($\theta_C = 45^\circ$). It is due to the fact that the polarization direction of the secondary beam,

$$\hat{\mathbf{e}}_S = \mathbf{k}_S \times (\mathbf{k}_S \times \hat{\mathbf{e}})/|\mathbf{k}_S \times (\mathbf{k}_S \times \hat{\mathbf{e}})|,$$

is the one that should be in the direction of the scattered beam, which in this case is the primary one ($\mathbf{k}_P$). Then, the condition for a polarization-forbidden coupling reflection is given by the relationship $|\lambda\mathbf{k}_P \cdot \hat{\mathbf{e}}_S| = 1$.

However, instead of just calculating the χ values for polarization-forbidden detour reflections, we prefer to use a more general concept. We have used the Born approximation to estimate how the polarization angle modulates the scattering from detour reflections. Since the wavefield from the detour reflection is proportional to

$$\mathbf{W} = \mathbf{k}_P \times \mathbf{k}_P \times [\mathbf{k}_S \times (\mathbf{k}_S \times \hat{\mathbf{e}})],$$

$M(\chi) = |\mathbf{W}|^2$ provides a good description of the intensity modulation by the polarization angle χ. Although it does not take into account the primary wavefield, the angle of the polarization-forbidden detour reflection, $\chi_{\rm pf}$, can be calculated for $M(\chi) = 0$.

3. Experimental

The experiments were carried out at the X-ray diffraction beamline of the National Synchrotron Light Source (LNLS), Brazil. With the beamline four-crystal monochromator (Tolentino & Rodrigues, 1992), the incident-beam wavelength was set to 1.49145 Å, checked by a similar procedure applied elsewhere (Morelhão *et al.*, 1998). For this wavelength, the Bragg angle of the {333} and {115} Si reflection families would be close to $\pi/4$, exactly 45.5197°. The choice of a short wavelength is important in order to reduce air absorption and to avoid vacuum paths in the experimental set-up. The horizontal divergence was limited by slits and the beam divergences were estimated from vertical and horizontal rocking curves of the 111 Si reflection as 9 and 23.8″, respectively. The intensity of the incident beam was monitored by the available

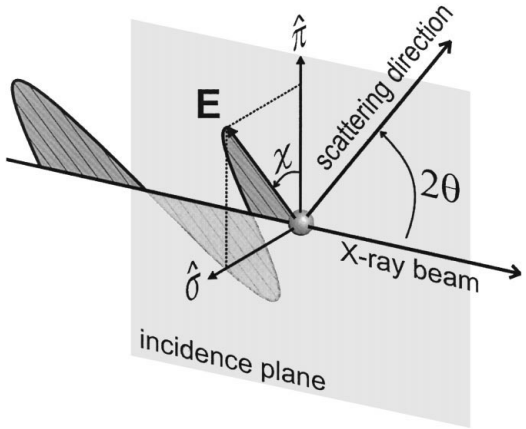

Figure 1
Coherent scattering of linearly polarized electromagnetic radiation by a free charge depends on the scattering angle 2θ as well as the polarization angle χ. Polarization-forbidden scattering directions occur when $2\theta = \pi/2$ and $\chi = 0$.

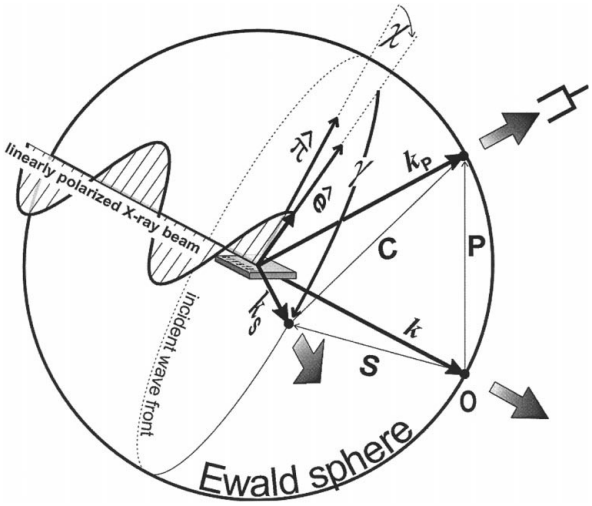

Figure 2
Reciprocal-space Ewald construction for a three-beam diffraction. **P**, **S** and **C = P − S** are the reciprocal vectors of the primary, secondary and coupling reflections. **k** stands for the wavevector of the incident linearly polarized X-ray beam, while $\mathbf{k}_P = \mathbf{P} + \mathbf{k}$ and $\mathbf{k}_S = \mathbf{S} + \mathbf{k}$ are the wavevectors of the diffracted beams. In this particular construction, $\mathbf{k}_S \cdot \mathbf{k} = 0$. A polarization-forbidden secondary reflection occurs when the polarization direction, $\hat{\mathbf{e}}$, is the same as $\mathbf{k}_S$.

ionization chamber, which provides a reference signal for normalizing the measured diffracted intensities.

A very simple and light three-axis goniometer (ω, φ and 2θ), also called ω:φ goniometer, was tightly fixed on top of a χ table, which was able to rotate the incidence plane of the goniometer from $\chi = -90$ to $+90^\circ$ in steps of 4°. $\chi = 0$ corresponds to the incidence plane in the horizontal position, and at $\chi = \pm 90^\circ$ it is vertical; $+$ and $-$ signs stand for the detector above and below the storage-ring horizontal plane, respectively. The minimum step sizes of the ω and φ axes are equal to 0.0004°.

4. Results

4.1. Renninger scan with polarization-forbidden primary reflection

Monitoring the intensity of the primary reflection while the crystal is rotated (φ rotation) around the diffraction vector of the primary reflection is well known as a Renninger scan (Renninger, 1937). Fig. 3 shows the Renninger scan performed with a polarization-forbidden primary reflection, which is in this case the 333 reflection of an Si [111] crystal. If the $[1\bar{1}0]$ crystal direction is taken as reference for the φ rotation, the peak at $\varphi = 0$ is due to the contribution of the $11\bar{1} + 224$ detour reflection. Its position does not depend on the wavelength so it was used as reference for the φ scale. The ω:φ scan of this peak as well as the φ scan with $\Delta\omega = 0$ are shown in the insets of Fig. 3. Table 1 gives the detour reflections for the 11 strongest peaks observed in this Renninger scan.

4.2. Detour reflection strength modulation

Several detour reflections in the Renninger scan of the very weak 222 Si primary reflection were investigated as a function of the polarization angle χ. Fig. 4 shows the detour reflection $31\bar{3} + \bar{1}15$ (D_1, $\varphi = 18.788^\circ$). Each φ scan in the figure was performed at the maximum of the primary reflection, verified by rocking curves (ω scans) for every different value of the polarization angle χ. The same procedure was carried out for other detour reflections, including $33\bar{3} + \bar{1}5\bar{1}$ (D_2, $\varphi = 17.999^\circ$), $11\bar{1} + 113$ (D_4, $\varphi = 5.485^\circ$) and $51\bar{1} + \bar{3}13$ (D_6, $\varphi = -2.988^\circ$). The measurements of D_1, D_2 and D_4 were carried out consecutively, before moving the χ table to its next position. Since it was a long time-consuming experiment, three shifts (time period of useful beam after each current injection at the LNLS storage ring) were necessary in order to complete

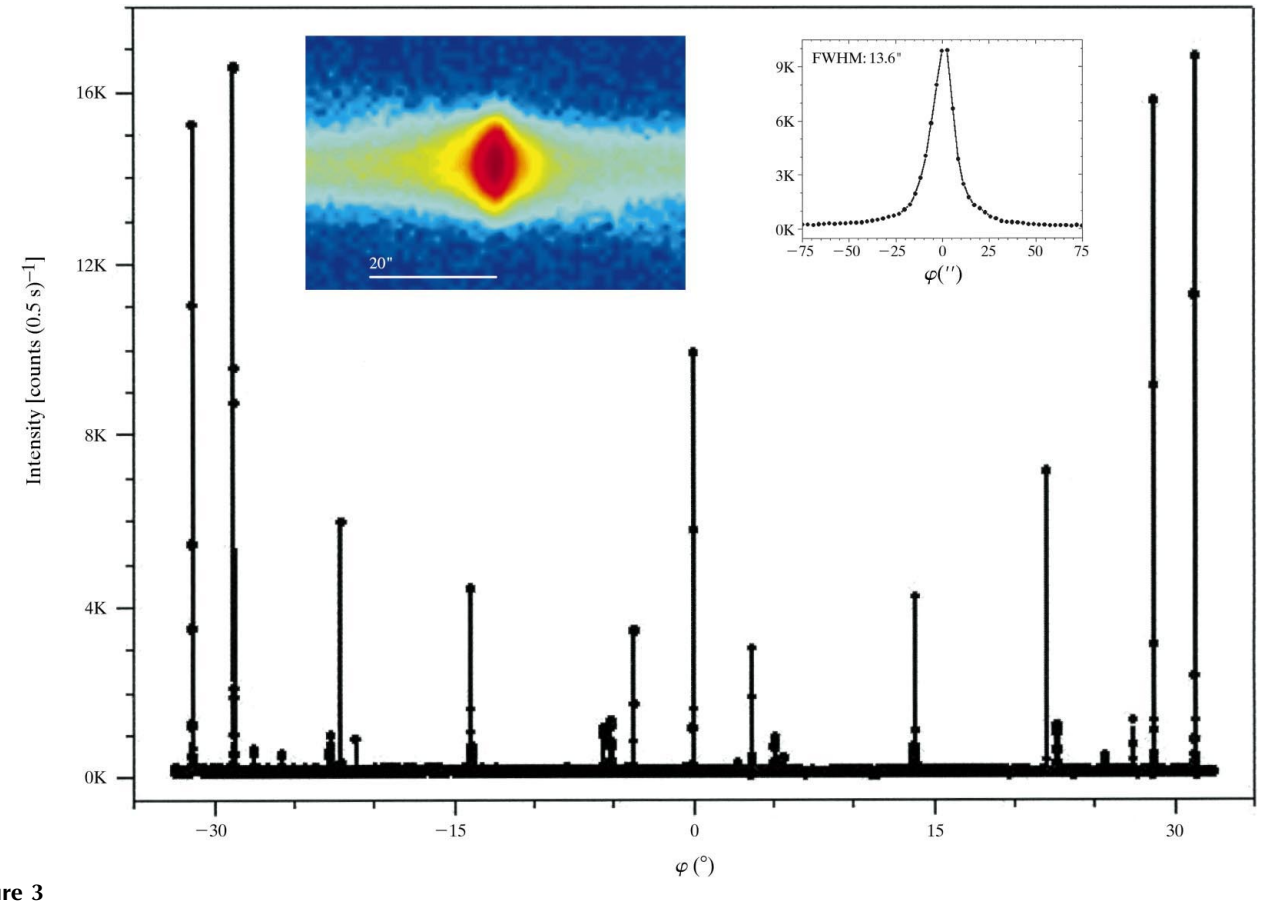

Figure 3
Renninger scan for a polarization forbidden primary reflection: π-polarized X-ray beam and Bragg angle of the 333 Si primary reflection near $\pi/4$. The step width of the scan is 0.0048°. The 11 strongest peaks are due to the detour reflections given in Table 1. The inset at the left-hand side is the ω:φ scan of the central peak. $\Delta\omega$ and $\Delta\varphi$ are the vertical and horizontal axes, respectively. The width of the φ-scan profile of this peak is shown in detail at the right-hand side.

Table 1
Detour reflections of the strongest peaks observed in the Renninger scan shown in Fig. 3.

The peaks with two detour reflections correspond to four-beam diffraction. $[1\bar{1}0]$ is the reference direction ($\varphi = 0$).

φ (°)	Detour reflections
−31.3123	$3\bar{1}\bar{1} + 044$ and $022 + 311$
−28.6877	$1\bar{1}3 + 440$ and $220 + 113$
−22.0347	$31\bar{1} + 024$
−13.8876	$004 + 33\bar{1}$ and $33\bar{1} + 002$
−3.6623	$31\bar{5} + 02\bar{2}$ and $0\bar{2}2 + 351$
0.0000	$11\bar{1} + 224$
3.6623	$531 + \bar{2}02$ and $20\bar{2} + 135$
13.8876	$33\bar{1} + 004$ and $002 + 331$
22.0347	$1\bar{1}3 + 240$
28.6877	$440 + \bar{1}\bar{1}3$ and $113 + 220$
31.3123	$404 + \bar{1}3\bar{1}$ and $131 + 202$

the set of measurements. For the last reflection, D_6, the φ scans were measured during only one shift.

The expected modulation of the maximum of the D_1 detour reflection intensity, as a function of χ, is given in Fig. 4 by the curve at $\Delta\varphi = 0$. This curve was generated by $M(\chi)$ and only its amplitude has been adjusted to the experimental data. The minimum scattering of the D_1, D_2 and D_6 reflections are observed in the φ scans performed at $\chi = 54$ (Fig. 4), ± 90 and $-66°$, respectively, and their maximum scattering at 90° from these values. The theoretical χ_{pf} values are 55.6, ± 90 and $-69.5°$, in the same order given above. For the D_1 reflection, as well as for the other measured detour reflections, some deviations of the experimental peak maximum intensities from the expected values have been observed. They are mostly due to misreading of the reference signal, and are minimized in the measurements of D_6 performed with shorter time intervals in between adjacent φ scans. In order to obtain a pattern for intensity comparison purposes, Fig. 5 shows the polarization direction effects on the ratios R_{14} and R_{24}, which are the maximum intensities of the D_1 (I_1) and D_2 (I_2) reflections divided by the intensity of the D_4 reflection (I_4), respectively, *i.e.* $R_{14} \equiv I_1/I_4$ and $R_{24} \equiv I_2/I_4$.

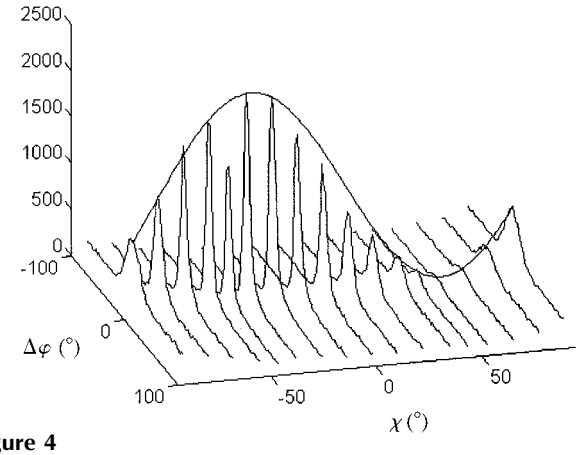

Figure 4
φ scans of the $31\bar{3} + \bar{1}15$ (D_1) detour reflection as a function of χ, the polarization direction of the incident X-ray beam. The scans were performed at $\chi = -90, -78, -66, -54, -45, -36, -24, -12, 0, 12, 24, 36, 45, 54, 66, 78, 90°$. The background intensity of the scans is due to the 222 Si primary reflection. The intensity scale is shown in counts per half second [counts $(0.5\ s)^{-1}$]. The minimum scattering of the detour reflection is seen at $\chi = 54°$, which is very close to the condition for a polarization-forbidden coupling reflection. $|\lambda \mathbf{k}_P \cdot \hat{\mathbf{e}}_S| = 1$ for $\chi = 55.6°$.

5. Relevance of the results and applications

One of the most interesting results is the Renninger scan of the polarization-forbidden primary reflection (Fig. 3). Besides the fact that each peak in the scan is an experimental observation of coherent scattering at $\pi/2$ of π-polarized photons, all detour reflections crystallographically allowed in the Renninger scan are seem as *Umweganregung*. This result obtained with synchrotron radiation is analogous to an experiment carried out 15 years ago (Kshevetskii *et al.*, 1985). In this experiment, the Renninger scan of the 333 Ge reflection with π-polarized Cu $K\alpha$ radiation was analyzed. Since then, multiple diffraction methods have found several applications in material analysis, such as the determination of piezoelectric coefficients of organic crystals (Avanci *et al.*, 1998), structural phase transitions in single-crystals (Avanci *et al.*, 2000), crystalline perfection of crystal surfaces (Morelhão & Cardoso, 1996; Hayashi *et al.*, 1997, Morelhão *et al.*, 1999) and precise lattice parameters of semiconductor heterostructures (Morelhão & Cardoso, 1993). All these applications, plus old applications such as the precise determination of lattice parameters of bulk crystals (Isherwood & Wallace, 1966; Post, 1975), are limited to the use of weak Bragg reflections as the primary one. Weak primary reflections allow measurement of the position and profiles of the detour reflections with better resolution. In the present situation, with the capability of tuning the wavelength at synchrotron facilities, the polarization-forbidden primary reflections open the fan of the above-mentioned applications of the multiple-diffraction phenomenon.

A limitation to a wide generalization of using such methods also resides in the fact that most diffractometers operating at

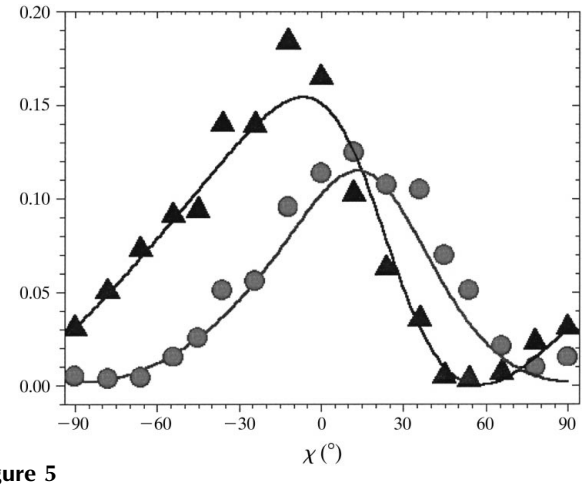

Figure 5
Intensity ratios as a function of the polarization direction. R_{14} (triangles) and R_{24} (circles) are the maximum intensities of the detour reflections D_1 (Fig. 4) and D_2 normalized by the intensity of D_4, respectively.

synchrotron stations have not been projected for a horizontal incidence-plane geometry. The experimental set-up with the ω:φ goniometer plus the χ table is a simple and inexpensive instrumental solution to overcome this difficulty. Moreover, the best resolution of the multiple diffraction peaks in φ scans is obtained with the primary incidence plane in the horizontal position ($\chi = 0$), as can be clearly seen from the ω:φ scan in the inset of Fig. 3. This experimental detail is relevant when the intensity of the synchrotron source does not allow the two divergences to be set at the same value without losing a significant amount of intensity.

The investigation of the detour reflection intensity modulation by the polarization angle provides experimental evidence that it can be described by the $M(\chi)$ function. And the polarization-forbidden detour reflections were observed at the predicted $\chi_{\rm pf}$ values of the polarization angle. Although the measurements were carried out with different vertical and horizontal incidence-beam divergences, it was not necessary to take it into account to adjust the modulation function to the experimental data. Both divergences are larger than the intrinsic widths of the multiple diffraction peaks. Then, for every position of the χ table, the divergences affect the peak widths but not the maximum peak intensities.

Detour reflections with $\mathbf{k}_S \cdot \mathbf{k} \approx 0$ or $\mathbf{k}_S \cdot \mathbf{k}_P \approx 0$ are very sensitive to the polarization direction, in the sense that their intensities can be completely eliminated from a Renninger scan for certain χ values. Such sensitivity can be applied in polarimetry, which is demonstrated here by the R_{14} (I_1/I_4) and R_{24} (I_2/I_4) intensity ratios plotted in Fig. 5. D_1 and D_2 reflections were chosen because they are very sensitive to the polarization direction and are forbidden for very distinct χ values. The D_4 reflection was taken since it has a relatively lower sensitivity; it is not forbidden for any χ. Consequently, the relative arrangement of the curves in Fig. 5 is unique and interesting. By analyzing these curves, it is possible to note that each pair of R_{14} and R_{24} values is assigned to only one χ value. For instance, $R_{24} \approx 0.05$ occurs for $\chi \approx -27$ and $\chi \approx 45^\circ$, but for these χ values R_{14} is close to 0.13 and 0.01, respectively, which are very different, bearing in mind the resolution of the measurements. Therefore, if the linear polarization state of an X-ray beam is unknown or must be experimentally verified (for example, with an insertion device), the measurements of the R_{14} and R_{24} ratios can provide an estimation. This procedure eliminates the necessity of using conventional X-ray polarimeters since the ratios can be extracted from one Renninger scan, even performed with the common geometry of a vertical incidence plane.

In summary, we have described by simple geometrical considerations and experimentally demonstrated that the polarization direction of synchrotron radiation is an important variable in multiple-diffraction phenomena. It can be explored to change the relative intensities of the primary and detour reflections. Acknowledgement of this fact is important since the applicability of the phenomenon in material analysis is limited to the multiple-diffraction cases in which the reflectivities of the primary and detour reflections match the desired conditions for each application.

Moreover, we showed a pattern for extracting the linear polarization state from intensity ratios of multiple diffraction peaks, which occurs in the Renninger scan of the 222 Si primary reflection.

The author would like to acknowledge L. P. Cardoso for participating and helping in the experiments. Thanks are due to C. Campos for useful discussions and to the LNLS for constructing the χ table. This work was supported by the Brazilian founding agencies FAPESP, grant nos. 97/13757–8 and 99/00046–1, and CNPq, proc. no. 301617/95–3.

References

Avanci, L. H., Cardoso, L. P., Girdwood, S. E., Pugh, D., Sherwood, J. N. & Roberts, K. J. (1998). *Phys. Rev. Lett.* **81**, 5426–5429.
Avanci, L. H., Cardoso, L. P., Girdwood, S. E., Sasaki, J. M., Roberts, K. J., Pugh, D. & Sherwood, J. N. (2000). *Phys. Rev. B*, **61**, 6507–6514.
Avanci, L. H. & Morelhão, S. L. (2000). *Acta Cryst.* A**56**, 507–508.
Caticha-Ellis, S. (1975). *Jpn. J. Appl. Phys.* **14**, 603–611.
Chang, S. L. (1982). *Phys. Rev. Lett.* **48**, 163–166.
Chang, S. L. (1984). *Multiple Diffraction of X-rays in Crystals.* Heidelberg: Springer-Verlag.
Chang, S. L. (1998). *Acta Cryst.* A**54**, 886–894.
Chang, S. L. & Tang, M. T. (1988). *Acta Cryst.* A**44**, 1065–1072.
Colella, R. (1974). *Acta Cryst.* A**30**, 413–423.
Hart, M. & Lang, A. R. (1961). *Phys. Rev. Lett.* **7**, 120–121.
Hayashi, M. A., Morelhão, S. L., Avanci, L. H., Cardoso, L. P., Sasaki, J. M., Kretly, L. C. & Chang, S. L. (1997). *Appl. Phys. Lett.* **71**, 2614–2616.
Isherwood, B. J. & Wallace, C. A. (1966). *Nature (London)*, **212**, 173–175.
Kshevetskii, S. A., Stetsko, Yu. P. & Shelud'ko, S. A. (1985). *Sov. Phys. Crystallogr.* **30**, 270–272.
Lipscomb, W. N. (1949). *Acta Cryst.* **2**, 193–194.
Moon, R. M. & Shull, C. G. (1964). *Acta Cryst.* **17**, 805–812.
Morelhão, S. L. & Abramof, E. (1999). *J. Appl. Cryst.* **32**, 871–877.
Morelhão, S. L., Avanci, L. H., Hayashi, M. A. & Cardoso, L. P. (1999). *Mater. Res. Soc. Proc.* **561**, 87–92.
Morelhão, S. L. & Cardoso, L. P. (1993). *J. Appl. Phys.* **73**, 4218–4226.
Morelhão, S. L. & Cardoso, L. P. (1996). *J. Appl. Cryst.* **29**, 446–456.
Morelhão, S. L., Hayashi, M. A., Avanci, L. H., Cardoso, L. P. & Collins, S. P. (1998). *Appl. Phys. Lett.* **73**, 2194–2196.
Post, B. (1975). *Acta Cryst.* A**31**, 153–155.
Post, B. (1977). *Phys. Rev. Lett.* **39**, 760–763.
Renninger, M. (1937). *Z. Kristallogr.* **97**, 107–121.
Shen, Q. & Collela, R. (1988). *Acta Cryst.* A**44**, 17–21.
Shen, Q. & Finkelstein, K. D. (1992). *Phys. Rev. B*, **45**, 5075–5078.
Shen, Q. & Finkelstein, K. D. (1993). *Rev. Sci. Instrum.* **64**, 3451–3455.
Stetsko, Yu. P., Juretschke, H. J., Huang, Y. S., Chao, C. H., Chen, C. K. & Chang, S. L. (2000). *Acta Cryst.* A**56**, 394–400.
Thorkildsen, G. (1987). *Acta Cryst.* A**43**, 361–369.
Tolentino, H. & Rodrigues, A. R. D. (1992). *Rev. Sci. Instrum.* **63**, 946–949.
Wagner, E. (1923). *Phys. Z.* **21**, 94–99.
Weckert, E. & Hümmer, K. (1997). *Acta Cryst.* A**53**, 108–143.